

# Spaceland Embedding of Sparse Stochastic Graphs

Nikos Pitsianis<sup>\*†</sup> Alexandros-Stavros Iliopoulos<sup>†</sup> Dimitris Floros<sup>\*</sup> Xiaobai Sun<sup>†</sup>

<sup>\*</sup>Department of Electrical and Computer Engineering  
Aristotle University of Thessaloniki  
Thessaloniki 54124, Greece

<sup>†</sup>Department of Computer Science  
Duke University  
Durham, NC 27708, USA

**Abstract**—We introduce a nonlinear method for directly embedding large, sparse, stochastic graphs into low-dimensional spaces, without requiring vertex features to reside in, or be transformed into, a metric space. Graph data and models are prevalent in real-world applications. Direct graph embedding is fundamental to many graph analysis tasks, in addition to graph visualization. We name the novel approach SG-t-SNE, as it is inspired by and builds upon the core principle of t-SNE, a widely used method for nonlinear dimensionality reduction and data visualization. We also introduce t-SNE-II, a high-performance software for 2D, 3D embedding of large sparse graphs on personal computers with superior efficiency. It empowers SG-t-SNE with modern computing techniques for exploiting in tandem both matrix structures and memory architectures. We present elucidating embedding results on one synthetic graph and four real-world networks. More experimental results and comparisons are in Supplementary Material.<sup>1</sup>

## I. INTRODUCTION

Big and sparse graph or network data exist and emerge in various research fields and real-world applications. Relational data of this type are in great diversity, such as biological networks, social, friend or co-author networks, commercial product networks, food webs, ecological networks, telecommunication networks, information networks, transportation networks, word co-occurrence networks, image-net, wordnet [1]–[15]. Graph/network analysis plays an important role in data analysis in general.

A graph  $\mathcal{G}(V, E)$  has a set  $V$  of vertices and a set  $E$  of edges. The vertices (nodes) are an abstraction of entities or objects that have concrete forms or possess particular attributes in a real-world context. The vertices may stand for molecules, proteins, neuron cells, species, products, customers, words, documents, signals or time series, images or pixels. An edge (link) connecting two vertices represents a certain relationship, an interaction, or proximity between them. Additional graph information may include vertex attributes and edge weights.

Fundamental to many graph analysis tasks, graph embedding renders a mapping from vertices to their coded vectors (abstract features) in a code space (the embedding space), with code length  $L$ . The mapping is subject to one or more conditions to preserve (or reconstruct) certain graph properties in the embedding space. If the edge weights indicate pairwise (geometric or geodesic) distances between nodes, one wishes to preserve the pairwise distances as much as possible. This type of graph embedding is vertex embedding. Often, the code

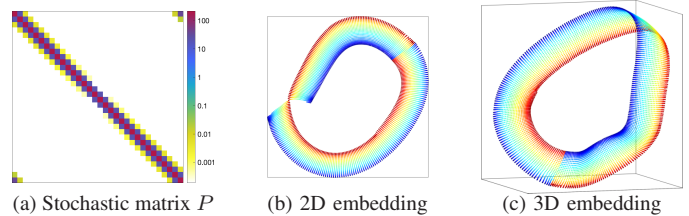


Fig. 1: Essential neighbor and structural connections in a  $k$ NN graph for a Möbius strip lattice, with  $n = 8,192 (= 256 \times 32)$  lattice nodes, are obscured or crumbled by a 2D embedding yet principally captured by a 3D embedding. (a) The stochastic matrix  $P$  of the  $k$ NN graph,  $k = 150$ , by Euclidean distance, is displayed in a  $32 \times 32$  pixel array. Each pixel represents a  $256 \times 256$  matrix block, its value (color coded) is the total sum of the block elements. (b)&(c) The embeddings are by SG-t-SNE with  $\lambda = 100$ , taking 1,000 iterations, including 250 early exaggeration ones with  $\alpha = 12$ . The initial coordinates are drawn from a random uniform distribution. The embedding of the same graph by the conventional t-SNE within the feasible perplexity range suffers more distortions, see Supplementary Material.

space for large graphs resides in  $\mathbb{R}^L$ , such as with `word2vec` and its variants [16], [17]. Various graph analysis tasks are subsequently carried out in an embedding space. They include (semi-, un-) supervised classification or stratification, abnormality detection, noise reduction, propagation patterns, content recommendation and other types of prediction. The feature vector length  $L$  is chosen sufficiently large for these multiple analytical tasks. In recent years, numerous types of high-dimensional graph embedding techniques are tried out with neural networks [18]–[28].

High-dimensional graph embedding is often followed and accompanied by dimension reduction and low-dimensional embedding for multiple purposes: (i) visual assessment, inspection and summary of the analysis results in large quantities; (ii) facilitating interactive exploration; and (iii) making connections to the original, interpretable attributes. There is a plethora of low-dimensional graph embedding techniques [29]–[32]. Most are distance-based, preserving geometric neighborhood, assuming vertex features in a metric space.

We make two major contributions in the present work. First, we introduce a novel nonlinear approach for directly embedding large, sparse, stochastic graphs into low-dimensional spaces, without requiring vertex features to reside in, or be transformed into, a metric space. There are a lot of stochastic graphs, in real-world applications, without feature vectors readily in a metric space or available for public use. Our approach, named SG-t-SNE, is inspired by and builds upon the

<sup>1</sup>Supplementary Material is at <http://t-sne-pi.cs.duke.edu>.

core principle of t-SNE, which is widely used for nonlinear dimensionality reduction and data visualization. There are many variants of t-SNE [33]–[40]. In SG-t-SNE, by a radical removal of the existing restrictions, we extend the use of t-SNE to the entire realm of stochastic graphs, no longer limited to distance-based  $k$ -nearest neighbor ( $k$ NN) graphs. SG-t-SNE is also equipped with a parameterized non-linear rescaling mechanism. It explores the sparsity to a much greater scope. In the case of a  $k$ NN graph, SG-t-SNE is capable of rendering much better embedding results than conventional t-SNE. See experimental comparisons in Supplementary Material.

Secondly, we introduce a software t-SNE-II. It accelerates 2D graph embedding up to  $5\times$  in execution time in comparison to the best among the existing t-SNE variants. More importantly, it enables 3D embedding of large sparse graphs on personal computers, with superior efficiency. We demonstrate in Fig. 1 that 3D embedding has greater capacity of preserving local and structural connectivity. Steerable visualization of all 3D embedding results is available at the online Supplementary Material. We present also experimental results on two biological networks, a social network created by Google, and an Amazon product network. The embedding results are characteristic and elucidating.

## II. EMBEDDING SPARSE STOCHASTIC GRAPHS

We introduce SG-t-SNE, with which we apply and extend the essential principle of t-SNE to the entire realm of sparse stochastic graphs. A stochastic graph  $\mathcal{G} = (V, E, \mathbf{P}_c)$  is associated with a stochastic weight matrix  $\mathbf{P}_c = [p_{j|i}]$ . At each vertex  $i$ ,  $\sum_j a_{ij} p_{j|i} = 1$ , where  $\mathbf{A} = [a_{ij}]$  is the binary-valued adjacency matrix (the sparsity mask) of the graph. We assume without loss of generality that  $\mathcal{G}$  has no isolated (0-degree) vertices. We are especially concerned with real-world graphs that have a large number of vertices and sparse connections ( $|E| = O(|V|)$ ). Real-world graphs do not necessarily have constant degrees.

### A. An investigative review of t-SNE

We describe first the essence of t-SNE. Provided with a graph  $\mathcal{G}$  with stochastic weights at each vertex, described by a stochastic matrix  $\mathbf{P}_c = (P_{j|i})$ , and given a prescribed modest dimensionality  $d$ , t-SNE generates vertex embedding coordinates  $\mathcal{Y}_d^* = \{\mathbf{y}_i\}_{i=1}^n$  in  $\mathbb{R}^d$ . With its configuration specified by the Student t-distribution  $\mathbf{Q}(\mathcal{Y}) = [q_{ij}]$ ,

$$q_{ij} = \frac{(1 + \|\mathbf{y}_i - \mathbf{y}_j\|^2)^{-1}}{\sum_{k \neq l} (1 + \|\mathbf{y}_k - \mathbf{y}_l\|^2)^{-1}}, \quad i \neq j, \quad (1)$$

the embedding arrives at the optimal matching to the joint distribution  $\mathbf{P} = (\mathbf{P}_c + \mathbf{P}_c^T)/2n$  in the sense that

$$\mathcal{Y}_d^* = \arg \min_{\mathcal{Y}} \text{KL}(\mathbf{P} \parallel \mathbf{Q}(\mathcal{Y})), \quad (2)$$

where KL denotes the Kullback-Leibler divergence.

The standard version of t-SNE, however, is developed, used, viewed and reviewed as a nonlinear dimension reduction algorithm, due primarily to the following interface to the distribution matching objective (2). The input is a set of data points

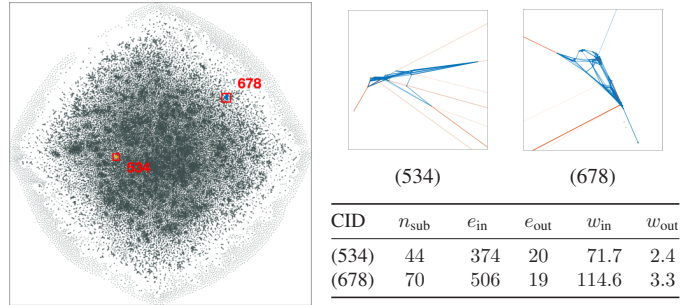


Fig. 2: Two-dimensional embedding of an Amazon product network, with  $n = 334,863$  products and  $m = 1,851,744$  edges, each edge represents connects two products that are frequently purchased together [41]. **Left:** Vertex embedding. The highlighted vertices are two disjoint product clusters with labels 534 and 678. The embedding is enabled by SG-t-SNE, with  $\lambda = 10$ , taking 8,000 iterations, including 2,000 early exaggeration iterations with  $\alpha = 12$ . The initial coordinates are drawn from a random Gaussian distribution. The graph is inadmissible to the conventional t-SNE. **Right:** The subgraphs of the two clusters with intra-edges in blue (close together) and external edges in red. The table details each of the clusters in numbers of nodes, internal edges and external edges, and the sum of weights over the internal and external edges. More scatterplots of the network are available in Supplementary Material.

in terms of feature vectors  $\mathcal{X} = \{\mathbf{x}_i\}_{i=1}^n$  in an  $L$ -dimensional space  $\mathbb{R}^L$  endowed with a distance function  $d(\cdot, \cdot)$ . The feature vector length  $L$  is (much) larger than the embedding dimension  $d$ . The algorithm locates the  $k$  nearest neighbors ( $k$ NN) of each vertex, and integrates them into the  $k$ NN graph, which is regular (with constant degree  $k$ ). Let  $\mathbf{A}$  be the binary-valued adjacency matrix. Denote by  $\mathbf{D}$  the matrix of squared pairwise distances,  $\mathbf{D} = [d_{ij}^2] = [d^2(\mathbf{x}_i, \mathbf{x}_j)]$ . Then, the distance-weighted  $k$ NN matrix  $\mathbf{D} \odot \mathbf{A}$  (Hadamard product) is converted to a stochastic matrix  $\mathbf{P}_c$  by parameterized exponentiation and normalization,

$$p_{j|i}(\sigma_i) = \frac{a_{ij} \exp(-d_{ij}^2/2\sigma_i^2)}{\sum_l a_{il} \exp(-d_{il}^2/2\sigma_i^2)}. \quad (3)$$

For every vertex  $i$ , the Gaussian parameter  $\sigma_i$  is determined by the equation

$$-\sum_j a_{ij} p_{j|i}(\sigma_i) \log(p_{j|i}(\sigma_i)) = \log(u), \quad (4)$$

where the prescribed perplexity  $u$  is a hyper-parameter. In fact, equation (4) equalizes all vertices by the conditional entropies.

We make a couple of remarks on the relationship between  $u$  and  $k$ . Commonly, the heuristic rule  $k = \lfloor 3u \rfloor$  is used. Veritably, the condition  $0 < u < k$  is necessary for the solutions to (4) to exist at all vertices. With a larger perplexity  $u$ , one would increase  $k$  proportionally to get a better embedding in the sense of (2), at the expense of a denser graph, larger memory requirement and longer execution time.

To unleash the greater potential with the essential t-SNE, we must unravel two elaborate restraining knots in the standard form. One is the coupling between distance and stochastics by (3). The other is the pairing between vertex degree and perplexity by (4).

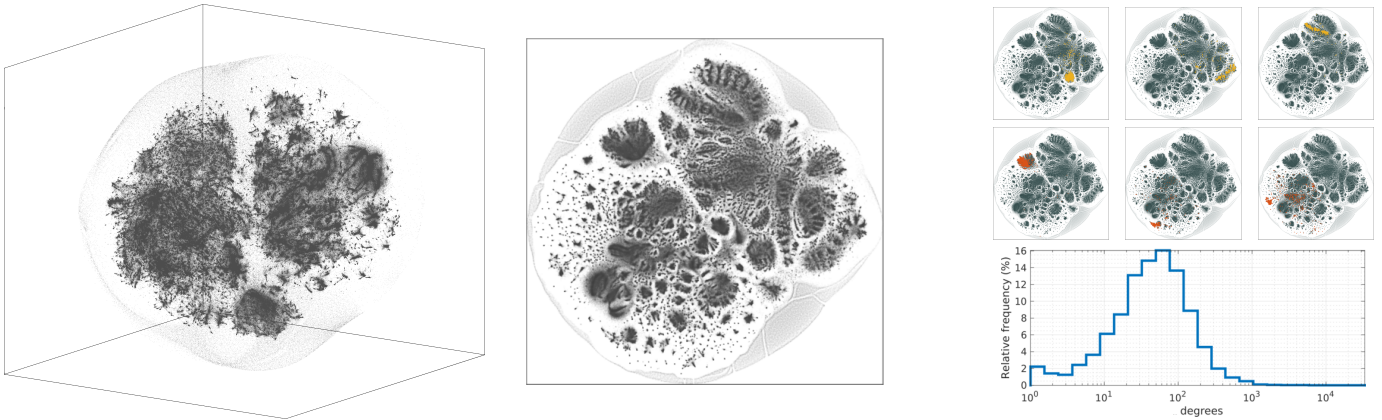


Fig. 3: Spaceland (3D) and Flatland (2D) embedding of the friend social network `orkut` as of 2012 [41]. The network has  $n = 3,072,441$  user nodes,  $m = 237,442,607$  friendship links. The degree varies from 1 (leaf nodes) to 33,313. The graph is not admissible to the conventional t-SNE. The embedding is by SG-t-SNE with  $\lambda = 10$ , taking 8,000 iterations, with initial coordinates drawn from a Gaussian random distribution. The 2D embedding takes only 50 minutes on the Xeon E5 (see Table I). **Left&Middle**: The vertex locations are structured, with entropy equal to 7.64. The leaf nodes (67,767 of them) are in the halo-like peripheral area. The rest can be roughly put into two hemispherical regions, which may likely correspond to the largest user populations in two geographical areas, one is in and around Brazil, the other is in and around India and some other countries in Asia. **Right**: The scatter diagrams in the thumbnails show six identified communities with labels 107, 325, 688 (top row) and 2196, 3208, 3405 (bottom row). The top ones reside in one hemispherical region; the bottom ones, in the other. This pattern indicates the impact of geographical regions, cultures and societies on social network structures.

### B. Advantages of admitting stochastic graphs

Stochastic graph data arise in numerous and various situations. Embedding of stochastic graphs will benefit network analysis and network-based data analysis in general.

The stochastic  $k$ NN graphs obtained by (3) and (4) are only a subset of stochastic graphs. While they play a key role for t-SNE being seen and used as a tool for nonlinear dimensionality reduction and data visualization on the one hand, they obscure the essential principle of t-SNE in several ways on the other hand. (i) Real-world graph data stem from various sources [1]–[4], [6]–[12], [41]. Often, the native and interpretable descriptors of the entity vertices are not readily in a metric space. The descriptors may contain both numerical and categorical data attributes. For such data, t-SNE may be preceded by a high-dimensional metric-space embedding, using machine learning tools (e.g., neural networks) and techniques [16], [17], as in parametrized t-SNE [42], at a very high computational cost. (ii) In the case where the feature descriptors are in a metric space, constructing the  $k$ NN graph is computationally expensive. Randomized methods are used to reduce the asymptotic complexity to  $O(n \log n)$  [43], [44]. However, such methods do not leverage domain-specific spaces of random variables [45]. (iii) The  $k$ NN graph and the outcome of t-SNE vary with the choice of vector space, distance function, and  $k$ NN search methods. (iv) The stochastic recasting of a  $k$ NN graph is exclusively confined in conventional t-SNE to the conditional Gaussian distribution, not inclusive of other probabilistic models. The above limitations are common to many t-SNE variants [33]–[40] and other multi-dimensional scaling (MDS) algorithms [29]–[31]. There exist nonlinear dimension reduction methods that attempt to circumvent the  $k$ NN search with certain sampling strategies [32].

Stochastic graphs are found or obtained in a multitude

of other ways. We give two examples. First, for high-security information networks, the vertex content features are not publicly accessible and their links are stochastically encrypted [46]. Second, network data are often available only with binary-valued links. Nonetheless, the stochastic weights of the links may be recovered to significant extent from the local neighborhood topologies and the global network topology. We use in this paper two such stochastic graphs from a recent study [47]: one is of a social network, the other of an e-commerce network. In addition, real-world graphs are typically irregular, with high-degree hub nodes and 1-degree leaf nodes. See for example the degree distribution of the social network in Fig. 3.

In short, with stochastic graphs, we effectively create a clear abstraction of distinguishing graph embedding from graph construction. We also establish an interface between the two key processes, disentangling them for integrating the best in each. We explore the deep potential of the t-SNE essence.

### C. Introduction of SG-t-SNE

Our algorithm SG-t-SNE follows the essential principle of t-SNE and removes the barriers in its conventional version. SG-t-SNE admits any stochastic graph  $\mathcal{G} = (V, E, \mathbf{P}_c)$ , including stochastic  $k$ NN graphs. SG-t-SNE is capable of not only adapting to the sparse pattern in the input, but also exploiting the pattern for better distribution matching and vertex embedding with a non-linear re-scaling mechanism.

Specifically, we generate from  $\mathbf{P}_c$  a parameterized family of stochastic matrices,  $\mathbf{P}_c(\lambda)$ , via nonlinear rescaling. The role of the rescaling mechanism is to explore and exploit the potential in distribution matching (2) from the  $\mathbf{P}$  side, given the fixed t-distribution (a Cauchy distribution) on the  $\mathbf{Q}$  side. Unlike the perplexity  $u$  in the conventional t-SNE, the parameter  $\lambda$  for SG-t-SNE exploits the sparsity without imposing any

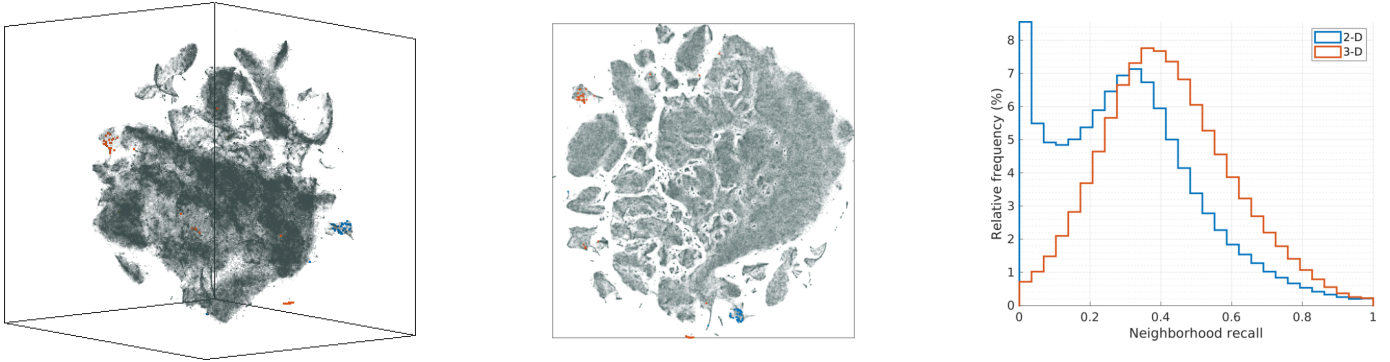


Fig. 4: Spaceland(3D) and Flatland(2D) embedding of the  $k$ NN graph ( $k = 90$ ) associated with  $n = 1,306,127$  RNA sequences of E18 mouse brain cells [48]. The  $k$ -neighbors ( $k = 90$ ) are located in the space of the 50 principle components of the top 1,000 variable genes [49]. **Left&Middle:** The embeddings are obtained by t-SNE-II with perplexity  $u = 30$ ; taking 8,000 iterations, including 2,000 early exaggeration iterations with  $\alpha = 12$ . The initial coordinates are drawn from a random uniform distribution. Two subpopulations are color annotated: GABAergic subtype (Sncg, Slc17a8) in blue and VLMC subtype (Spp1, Coll15a1) in red. They are clearly separated from the rest in 3D embedding, see steerable 3D rendering in Supplementary Material. **Right:** Histograms of the stochastic  $k$ -neighbors recall values at all vertices,  $\text{recall}(i) = \sum_j \mathbf{P}_{j|i} b_{ij}$ , where  $\mathbf{B}_k = [b_{ij}]$  is the adjacency matrix of the  $k$ NN graph of the embedding points  $\{\mathbf{y}_i\}$ , in Euclidean distance. The stochastic weights  $p_{j|i}$  are common to both 2D and 3D embedding. The histogram for the 3D embedding (in red) shows relatively higher recall scores in larger cell population. The quantitative comparison is consistent with that by visual inspection.

constraint. In the special case of a weighted  $k$ NN graph,  $\lambda$  is untangled from  $k$ .

We describe the mechanism and effect of nonlinear rescaling with a single parameter  $\lambda$ . Let  $\phi(\cdot)$  be a rescaling kernel function that is monotonically increasing over  $\mathbb{R}_+$ , with  $\phi(0) \geq 0$ . For any  $\lambda > 0$ , SG-t-SNE generates  $\mathbf{P}_c(\lambda)$  as follows. Let  $\mathbf{A}$  be the binary-valued adjacency matrix (i.e., the sparsity mask) of graph  $\mathcal{G}$ , which is invariant to any change in  $\phi$  or  $\lambda$ . We determine the rescaling exponent  $\gamma_i$  at each vertex  $i$  by the equation

$$\sum_j a_{ij} \phi(p_{j|i}^{\gamma_i}) = \lambda, \quad (5)$$

and then reshape and rescale the conditional probability

$$p_{j|i}(\lambda) = \frac{a_{ij} \phi(p_{j|i}^{\gamma_i})}{\lambda}. \quad (6)$$

Unlike (4), the rescaling solutions exist unconditionally.

The rescaling mechanism introduces an additional degree of freedom to exploit the sparsity in an arbitrary form. In particular, we use the identity function  $\phi(x) = x$  as the rescaling kernel for the experiments presented in this paper. At  $\lambda = 1$  we get  $\gamma_i = 1$  and  $\mathbf{P}_c(1) = \mathbf{P}_c$ , the input matrix. At an integer value  $\lambda = k > 1$ , if  $\text{degree}(\ell) = k$ , then  $\gamma_\ell = 0$  and  $p_{j|\ell} = 1/k$ . In the special case of a regular graph with degree  $k$ , if we set  $\lambda = k$ , then  $\gamma_i = 0$  at all vertices, i.e.,  $\mathbf{P}_c(k) = \mathbf{A}/k$ . In general, at  $\lambda \neq 1$ , the ratio between every nonzero element to the peak element ( $p_{j|i}/\max_l p_{l|i}$ ) is changed to  $(p_{j|i}/\max_l p_{l|i})^{\gamma_i}$ . The weight distribution for each vertex is re-shaped, according to the re-scaling equation (5), in autonomous adaptation to the local sparsity.

In implementation, only two changes are made from the conventional version. One is at the interface, which takes either a distance-based  $k$ NN graph as in the conventional t-SNE or a stochastic matrix directly. The other is the change from the perplexity equation (4) to the rescaling equation (6).

We show in Figs. 2 and 3 the embeddings of two real-world networks, enabled by SG-t-SNE. Each exhibits a distinctive cluster structure. We show in Fig. 5 that even with  $k$ NN graphs at input, the embedding by t-SNE at  $k = 150$ ,  $u = 50$  is matched or outperformed by that with SG-t-SNE at  $k = 90$ ,  $\lambda = 10$ , on a sparser matrix and at a lower computation cost. We recommend multiple views at various values of  $\lambda$ .

### III. RAPID SPACELAND EMBEDDING

The practical use of t-SNE is largely confined to Flatland (2D) or Lineland (1D) embedding, despite the prototype implementation by van der Maaten<sup>2</sup> supporting embedding in several dimensions. We advocate Spaceland (3D or higher) embedding. Among abundant evidence, we illustrate in Figs. 1, 3, and 4, the extended capacity to capture and reveal multi-fold connections between (overlapping) subpopulations. With Spaceland embedding, we endorse “the enlargement of the imagination” [50].

There were multiple obstacles to Spaceland embedding. The journey of t-SNE is marked by continuous efforts and progress in reducing the arithmetic complexity and execution time of searching for an optimal embedding. We present t-SNE-II, a software renovation, a new milestone in performance. It enables rapid Spaceland embedding of large sparse graphs on modern desktop or laptop computers, which are available and affordable to researchers by and large.

The embedding coordinates, i.e.,  $dn$  parameters, are determined by t-SNE via applying the gradient descent method to the minimization problem (2). The computation per iteration step is dominated by the calculation of the gradient, which is reformulated in two terms by van der Maaten [35],

$$\frac{\partial(\text{KL})}{\partial \mathbf{y}_i} = \underbrace{\frac{4}{Z} \sum_{i \neq j} p_{ij} q_{ij} (\mathbf{y}_i - \mathbf{y}_j)}_{\text{attractive term}} - \underbrace{\frac{4}{Z} \sum_{i \neq j} q_{ij}^2 (\mathbf{y}_i - \mathbf{y}_j)}_{\text{repulsive term}}, \quad (7)$$

<sup>2</sup><https://lvdmaaten.github.io/tsne>

where  $Z = \sum_{ij} q_{ij}$ . The terms are named by analogy to the attractive and repulsive forces in molecular dynamics simulations. The attractive term can be cast as the sum of multiple matrix-vector products with a sparse matrix  $\mathbf{PQ} = [p_{ij}q_{ij}]$  and  $d$  coordinate vectors, one along each embedding dimension. Similarly, the repulsive term can be cast as the sum of multiple matrix-vector products with a dense matrix  $\mathbf{QQ} = [q_{ij}q_{ij}]$  and  $d$  coordinate vectors. The calculation of the attractive term takes  $O(dm)$  arithmetic operations, where  $m = |E|$  is the number of edges. A naive calculation of the repulsive term takes  $O(dn^2)$  arithmetic operations. This quadratic complexity would prohibit the use of t-SNE with large graphs.

### A. Fast approximations to the repulsive term

Two existing t-SNE variants use approximate algorithms to calculate the repulsive term. They reduce the quadratic complexity to  $O(c^d(\epsilon^{-1})n \log(n))$ , where  $c(\epsilon^{-1}) > 2$  increases reciprocally with  $\epsilon$ , a prescribed approximation error tolerance. The specific value of  $c$  in the prefactor  $c^d$  depends also on the choice of approximation algorithm and its parameters. The first approximation algorithm, by van der Maaten, adopts the tree code based on the Barnes-Hut (BH) algorithm [51]. We refer to this version as t-SNE-BH. An alternative approximation algorithm, named FIt-SNE, emerged last year [40].

We describe the fundamental concepts and distinctive approaches behind the two approximation algorithms, instead of reviewing each in detail. The matrix-vector multiplication with  $\mathbf{QQ}$  is a convolution with the Cauchy kernel on non-equispaced, scattered data points  $\{y_i\}_{i=1}^n$ . We refer to such a convolution as “nuConv”. A convolution may have broad or narrow (windowed) support. Narrow-support convolution has complexity  $O(wn)$ , where  $w$  is the bandwidth or support window size; the corresponding matrix is sparse and banded. The nuConv with  $\mathbf{QQ}$  is of broad support and dense. Fortunately, the matrix structure can be exploited.

There are two renowned and distinctive families of algorithms for fast nuConv of broad support. One family is based on the fast multipole method (FMM), with asymptotic arithmetic complexity  $O(n)$  [52]–[54]. FMM splits a convolution of broad support into  $O(\log(n))$  convolutions of narrow supports at multiple spatial levels. Its extended family includes the Barnes-Hut algorithm, with complexity  $O(n \log(n))$  [51]. The other family is based on non-uniform fast Fourier transforms (nuFFT), with arithmetic complexity  $O(n \log(n))$  [21], [55]. FIt-SNE takes the latter approach.

FIt-SNE is available for 1D/2D embedding only. By a careful comparison, its arithmetic complexity is lower than t-SNE-BH at the same accuracy level. Nonetheless, the execution time for 2D embedding with FIt-SNE (or t-SNE-BH) is now dominated by the computation of the attractive term; see Fig. 6. Furthermore, both FIt-SNE and t-SNE-BH face a steep rise in execution time for 3D embedding. FIt-SNE also suffers from exponential growth in memory demand due to zero padding for explicit conversion to periodic convolution.

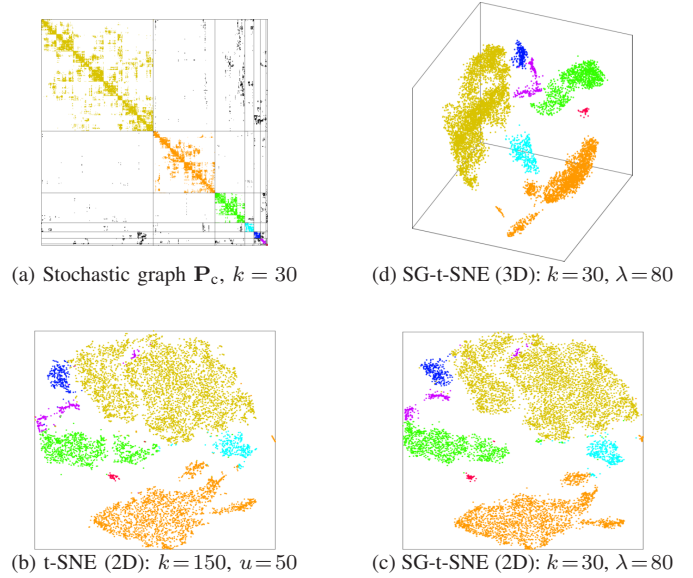


Fig. 5: Multiple views of subpopulations of  $n = 8,381$  peripheral blood mononuclear cells (PBMC-8k) [49]. The subpopulations (color-coded) were found by the SD-DP classification analysis [56]. (a) The stochastic  $k$ NN graph  $\mathbf{P}_c$  ( $k = 30$ ), with rows/columns permuted so that cells in the same subpopulation are placed together. Each pixel corresponds to a  $16 \times 16$  matrix block. (b)&(c) It is compelling that the embedding by SG-t-SNE on a sparse graph is comparable to that by t-SNE on a graph  $5 \times$  as dense. (d) Rapid Spaceland (3D) embedding is enabled by t-SNE-II, steerable view available in Supplementary Material. All three embeddings take 1,000 iterations, including 250 early exaggeration iterations with  $\alpha = 12$ , the initial embedding coordinates are drawn from uniformly random distribution.

### B. Introduction of t-SNE-II

With t-SNE-II, we advance the entire gradient calculation of (7) and enable Spaceland (3D) embedding in shorter time than Flatland (2D) embedding with FIt-SNE or t-SNE-BH. We overcome challenges at multiple algorithmic stages with innovative approaches. We utilize the matrix structure and the memory architecture in concert.

We not only expedite further the repulsive term computation with dense matrix  $\mathbf{QQ}$ , but also accelerate the attractive term computation with sparse matrix  $\mathbf{PQ}$ . Furthermore, we make swift translocation of  $\{y_i\}$  between the two terms.

*Fast computation with  $\mathbf{QQ}$ :* We take the spectral approach, similar to FIt-SNE. Set first an equispaced grid  $G$  in the spatial embedding domain. The nuConv with  $\mathbf{QQ}$  is then factored into three consecutive convolutional operations which we code-name as S2G, G2G and, G2S. The S2G and G2S convolutions translate  $\{y_i\}$  to their neighboring grid points, and vice versa. G2S is instrumented as a local interpolation and S2G is its transpose. Both are of narrow support, with arithmetic complexity  $O(w^d n)$ , where  $w$  is the interpolation window size per side. Factor G2G is a non-periodic convolution across the grid  $G$ .

We make algorithmic innovations for each of the factor convolutions. Instead of explicit embedding G2G into a circulant one as in FIt-SNE, we use an implicit approach without augmenting the grid size and its memory usage by a factor

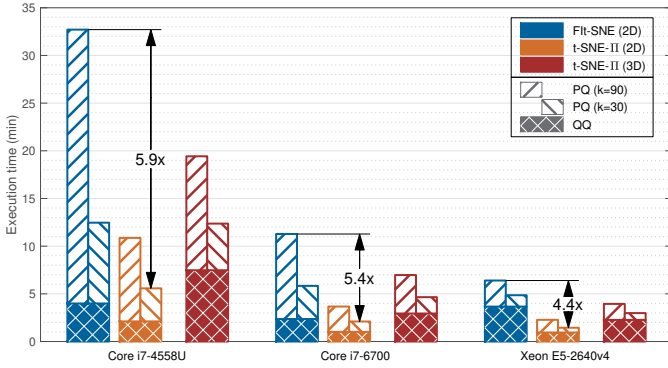


Fig. 6: Multiple comparisons in execution time for embedding of  $k$ NN graphs,  $k \in \{30, 90\}$ , with 1,306,127 nodes as single-cell RNA sequences of E18 mouse brain cells [48]. Each embedding takes 1,000 iterations and maintains below the same tolerance ( $10^{-6}$ ) on approximation errors. (a) In total time, with the same sparsity parameter  $k$ , 3D embeddings by t-SNE-II take less time to finish  $1.5\times$  operations in comparison to 2D embeddings by t-SNE, on each of the three multi-core computers used. (b) In memory usage, t-SNE-II does not augment grid size and thereby admits larger graphs. (c) The computation with sparse matrix **PQ** dominates the t-SNE time on machines with lower bandwidth, see Table I. SG-t-SNE reduces the PQ time further ( $5\times$  on Core i7-6700) by embedding a sparse graph ( $k = 30$ ) with results comparable to that by t-SNE on the graph  $3\times$  as dense. Additional notes: the t-SNE-II code is to be optimized; a version utilizing graphics card, if any, is in development.

of  $2^d$ , while maintaining the same arithmetic complexity. This memory saving allows a laptop or desktop computer to admit larger graphs. The factors S2G and G2S prolong the execution time due to irregular data access, a typical challenge in sparse matrix calculation. We introduce a dual grid  $G_{\text{dual}}$  for gridding the scattered data points  $\{y_i\}$ . Prior to S2G, the scattered points are binned into the dual-grid cells. Then, S2G translates the gridded data on  $G_{\text{dual}}$  to grid  $G$ , on which  $G2G$  takes place. This approach significantly improves the data locality and parallelism scope in S2G, and shortens the S2G time, accounting for the gridding overhead. The same holds true for G2S. We omit implementation details.

*Fast computation with PQ:* Irregular sparse pattern of **PQ** invokes irregular memory accesses which incur long latency on modern computers with hierarchical memories [57]. The execution time of Fit-SNE is evidently dominated by the computation with **PQ** at  $k = 90$  and  $u = 30$ ; see Fig. 6. The CPU is frequently in data-hungry state, the computation speed is limited by the memory bandwidth.

We mitigate the problem with a preprocessing step, based on the fact that matrix **PQ** inherits the fixed sparsity of matrix **P**, despite the dense structure and dynamic change of **Q**. We permute **P** such that similar rows and columns are clustered and placed together. The permuted matrix becomes block-sparse with denser blocks (BSDB), not necessarily block diagonal. A denser block implies higher data locality in memory reads and writes. We employ several efficient ways for clustering rows and columns (symmetrically). For a  $k$ NN graph at input, in particular, t-SNE-II has options among PCA-based cluster analysis and the SD-DP classification analysis [56]. The permutation overhead is amortized across all iterations. It is well paid off; see Fig. 6.

TABLE I: Architecture specification of three multi-core computers used for the embedding experiments. Memory bandwidth is measured with the parallel STREAM copy benchmark [60].

CPU	Clock (GHz)	Cores	L1	L2	L3	RAM	BW
			(KiB)	(KiB)	(MiB)	(GiB)	(GiB/s)
			per-core		shared		
Intel Core i7-4558U	2.80	2	64	256	4	8	10.5
Core i7-6700	3.40	4	32	256	8	32	19.9
Xeon E5-2640v4*	2.40	10	32	256	25	256	36.7

\*2 sockets (non-uniform memory access—NUMA)

In implementation detail, we adopt the storage format and sparse matrix computation routines provided in the Compressed Sparse Blocks (CSB) library [58], [59].

*Fast data translocation:* The embedding coordinate data  $\{y_i\}$  undergo dynamic change during the process of iterative search and matching (2). They are accessed in the computation with both **QQ** and **PQ**, but in different orderings. Matrix **P**, and hence **PQ**, is permuted, once for all, by row/column clusters. The order  $\{y_i\}$  is accessed in the computation with **QQ**, is determined by the dual-grid cells for S2G and G2S. At each iteration step, we translocate the data  $\{y_i\}$ , back and forth between the two terms, in multiple stages. In essence, a point-to-point cross permutation is factored into layers of block-to-block permutations.

We use **II** in the name of t-SNE-II to signify the role of permutations, factored permutation and the rational behind. Permutations are unaccounted for in arithmetic complexity. They play, however, the key role of making the algorithm and its building blocks attuned to the memory hierarchy. Without this harmonious algorithm-architecture mapping, memory access latency typically dominates the execution time in computation with large, sparse or compressible matrices [61], [62].

#### IV. ADDITIONAL REMARKS

The embedding results obtained by SG-t-SNE, powered by t-SNE-II, are elucidating. The embedding results with `orkut` and `Amazon` show clearly distinctive cluster or communities patterns. Furthermore, we find overlapping and non-overlapping regions between communities in `orkut`. The embedding of `Amazon` may serve as a map for market study and analysis, in assessing previous claimed product clusters and making new hypotheses or predictions. Even with  $k$ NN graphs, 3D embedding liberates us from 2D confinement and takes us to a deeper space where we can see multiple views at once, discover previously unseen connections and separations, such as with the PBMCs data and the E18-MBCs data. Additionally, we bring out the fascinating beauty of `orkut` and `Amazon` in their respective embedding spaces.

#### ACKNOWLEDGMENTS

We thank Tiancheng Liu for providing the sparse and stochastic graphs for the `orkut` and `Amazon` networks. We thank Pantazis Vouzaksakis and Xenofon Theodoridis for their assistance with the experiments.

## REFERENCES

- [1] R. Albert, H. Jeong, and A.-L. Barabási, "Diameter of the world-wide web," *Nature*, vol. 401, no. 6749, pp. 130–131, 1999.
- [2] M. Girvan and M. E. Newman, "Community structure in social and biological networks," *Proceedings of the National Academy of Sciences*, vol. 99, no. 12, pp. 7821–7826, 2002.
- [3] J. Kunegis, "KONECT: The koblenz network collection," in *Proceedings of the 22nd International Conference on World Wide Web*, 2013, pp. 1343–1350.
- [4] H. Kwak, C. Lee, H. Park, and S. Moon, "What is Twitter, a social network or a news media?" in *Proceedings of the 19th International Conference on World Wide Web*, 2010, pp. 591–600.
- [5] J. Yang and J. Leskovec, "Defining and evaluating network communities based on ground-truth," *Knowledge and Information Systems*, vol. 42, no. 1, pp. 181–213, 2015.
- [6] M. Cha, H. Haddadi, F. Benevenuto, and K. P. Gummadi, "Measuring user influence in Twitter: the million follower fallacy," in *Proceedings of the 4th International AAAI Conference on Weblogs and Social Media*, 2010.
- [7] M. E. Newman, "Finding community structure in networks using the eigenvectors of matrices," *Physical Review E*, vol. 74, no. 3, p. 036104, 2006.
- [8] S. Auer, C. Bizer, G. Kobilarov, J. Lehmann, R. Cyganiak, and Z. Ives, "DBpedia: A nucleus for a web of open data," in *The Semantic Web*, 2007, pp. 722–735.
- [9] H. Yu, P. Braun, M. A. Yildirim, I. Lemmens, K. Venkatesan, J. Sahalie, T. Hirozane-Kishikawa, F. Gebreab, N. Li, N. Simonis, T. Hao, J.-F. Rual, A. Dricot, A. Vazquez, R. R. Murray, C. Simon, L. Tardivo, S. Tam, N. Svrzikapa, C. Fan, A.-S. de Smet, A. Motyl, M. E. Hudson, J. Park, X. Xin, M. E. Cusick, T. Moore, C. Boone, M. Snyder, F. P. Roth, A.-L. Barabási, J. Tavernier, D. E. Hill, and M. Vidal, "High-quality binary protein interaction map of the yeast interactome network," *Science*, vol. 322, no. 5898, pp. 104–110, 2008.
- [10] S. Redner, "Citation statistics from more than a century of Physical Review," 2004, arXiv:physics/0407137 [physics.soc-ph].
- [11] W. W. Zachary, "An information flow model for conflict and fission in small groups," *Journal of Anthropological Research*, vol. 33, no. 4, pp. 452–473, 1977.
- [12] D. J. Watts and S. H. Strogatz, "Collective dynamics of 'small-world' networks," *Nature*, vol. 393, no. 6684, pp. 440–442, 1998.
- [13] O. Russakovsky, J. Deng, H. Su, J. Krause, S. Satheesh, S. Ma, Z. Huang, A. Karpathy, A. Khosla, M. Bernstein, A. C. Berg, and L. Fei-Fei, "ImageNet large scale visual recognition challenge," *International Journal of Computer Vision*, vol. 115, no. 3, pp. 211–252, 2015.
- [14] G. A. Miller, "WordNet: a lexical database for English," *Communications of the ACM*, vol. 38, no. 11, pp. 39–41, 1995.
- [15] C. Fellbaum, *WordNet: an electronic lexical database*. MIT press, 1998.
- [16] T. Mikolov, I. Sutskever, K. Chen, G. Corrado, and J. Dean, "Distributed representations of words and phrases and their compositionality," in *Advances in Neural Information Processing Systems*, vol. 26, 2013, pp. 3111–3119.
- [17] J. Pennington, R. Socher, and C. D. Manning, "GloVe: global vectors for word representation," in *Empirical Methods in Natural Language Processing*, 2014, pp. 1532–1543.
- [18] M. A. Kramer, "Nonlinear principal component analysis using autoassociative neural networks," *AIChE journal*, vol. 37, no. 2, pp. 233–243, 1991.
- [19] B. Fritzsche, "A growing neural gas network learns topologies," in *Advances in neural information processing systems*, 1995, pp. 625–632.
- [20] G. E. Hinton and R. R. Salakhutdinov, "Reducing the dimensionality of data with neural networks," *science*, vol. 313, no. 5786, pp. 504–507, 2006.
- [21] W. Wang, Y. Huang, Y. Wang, and L. Wang, "Generalized autoencoder: A neural network framework for dimensionality reduction," in *Proceedings of the IEEE Conference on Computer Vision and Pattern Recognition Workshops*, 2014, pp. 490–497.
- [22] J. Tang, M. Qu, M. Wang, M. Zhang, J. Yan, and Q. Mei, "LINE: large-scale information network embedding," in *Proc. WWW*, 2015, pp. 1067–1077.
- [23] J. H. Levine, E. F. Simonds, S. C. Bendall, K. L. Davis, E.-a. D. Amir, M. D. Tadmor, O. Litvin, H. G. Fienberg, A. Jager, E. R. Zunder, R. Finck, A. L. Gedman, I. Radtke, J. R. Downing, D. Pe'er, and G. P. Nolan, "Data-driven phenotypic dissection of AML reveals progenitor-like cells that correlate with prognosis," *Cell*, vol. 162, no. 1, pp. 184–197, 2015.
- [24] A. Klein, L. Mazutis, I. Akartuna, N. Tallapragada, A. Veres, V. Li, L. Peshkin, D. Weitz, and M. Kirschner, "Droplet barcoding for single-cell transcriptomics applied to embryonic stem cells," *Cell*, vol. 161, no. 5, p. 1187–1201, May 2015.
- [25] I. Tirosh, B. Izar, S. M. Prakadan, M. H. Wadsworth, D. Treacy, J. J. Trombetta, A. Rotem, C. Rodman, C. Lian, G. Murphy, M. Fallahi-Sichani, K. Dutton-Regester, J.-R. Lin, O. Cohen, P. Shah, D. Lu, A. S. Genshaft, T. K. Hughes, C. G. K. Ziegler, S. W. Kazer, A. Gaillard, K. E. Kolb, A.-C. Villani, C. M. Johannessen, A. Y. Andreev, E. M. Van Allen, M. Bertagnoli, P. K. Sorger, R. J. Sullivan, K. T. Flaherty, D. T. Frederick, J. Jané-Valbuena, C. H. Yoon, O. Rozenblatt-Rosen, A. K. Shalek, A. Regev, and L. A. Garraway, "Dissecting the multicellular ecosystem of metastatic melanoma by single-cell RNA-seq," *Science*, vol. 352, no. 6282, pp. 189–196, 2016.
- [26] B. Becher, A. Schlitzer, J. Chen, F. Mair, H. R. Sumatoh, K. W. W. Teng, D. Low, C. Ruedl, P. Riccardi-Castagnoli, M. Poidinger, M. Greter, F. Ginhoux, and E. W. Newell, "High-dimensional analysis of the murine myeloid cell system," *Nature Immunology*, vol. 15, no. 12, pp. 1181–1189, 2014.
- [27] M. M. Bronstein, J. Bruna, Y. LeCun, A. Szlam, and P. Vandergheynst, "Geometric deep learning: going beyond Euclidean data," *IEEE Signal Processing Magazine*, vol. 34, no. 4, p. 18–42, 2017.
- [28] K. Cho, B. van Merriënboer, C. Gulcehre, D. Bahdanau, F. Bougares, H. Schwenk, and Y. Bengio, "Learning phrase representations using RNN encoder-decoder for statistical machine translation," in *Proc. EMNLP*, 2014, pp. 1724–1734.
- [29] A. Mead, "Review of the development of multidimensional scaling methods," *Journal of the Royal Statistical Society: Series D (The Statistician)*, vol. 41, no. 1, pp. 27–39, 1992.
- [30] Y.-H. Fua, M. O. Ward, and E. A. Rundensteiner, "Hierarchical parallel coordinates for exploration of large datasets," in *Proceedings of the Conference on Visualization '99: Celebrating Ten Years*, 1999, pp. 43–50.
- [31] J.-J. Huang, G.-H. Tzeng, and C.-S. Ong, "Multidimensional data in multidimensional scaling using the analytic network process," *Pattern Recognition Letters*, vol. 26, no. 6, pp. 755–767, 2005.
- [32] L. McInnes, J. Healy, and J. Melville, "UMAP: Uniform manifold approximation and projection for dimension reduction," 2018, arXiv:1802.03426 [stat.ML].
- [33] L. van der Maaten and G. Hinton, "Visualizing data using t-SNE," *Journal of Machine Learning Research*, vol. 9, no. Nov, pp. 2579–2605, 2008.
- [34] E.-a. D. Amir, K. L. Davis, M. D. Tadmor, E. F. Simonds, J. H. Levine, S. C. Bendall, D. K. Shenfeld, S. Krishnaswamy, G. P. Nolan, and D. Pe'er, "viSNE enables visualization of high dimensional single-cell data and reveals phenotypic heterogeneity of leukemia," *Nature Biotechnology*, vol. 31, no. 6, pp. 545–552, 2013.
- [35] L. van der Maaten, "Accelerating t-SNE using tree-based algorithms," *Journal of Machine Learning Research*, vol. 15, no. Oct, pp. 3221–3245, 2014.
- [36] W. M. Abdelmoula, B. Balluff, S. Englert, J. Dijkstra, M. J. T. Reinders, A. Walch, L. A. McDonnell, and B. P. F. Lelieveldt, "Data-driven identification of prognostic tumor subpopulations using spatially mapped t-SNE of mass spectrometry imaging data," *Proceedings of the National Academy of Sciences*, vol. 113, no. 43, pp. 12 244–12 249, 2016.
- [37] N. Pezzotti, T. Höllt, B. Lelieveldt, E. Eisemann, and A. Vilanova, "Hierarchical stochastic neighbor embedding," *Computer Graphics Forum*, vol. 35, no. 3, pp. 21–30, 2016.
- [38] N. Pezzotti, B. P. F. Lelieveldt, L. van der Maaten, T. Höllt, E. Eisemann, and A. Vilanova, "Approximated and user steerable tSNE for progressive visual analytics," *IEEE Transactions on Visualization and Computer Graphics*, vol. 23, no. 7, pp. 1739–1752, 2017.
- [39] V. van Unen, T. Höllt, N. Pezzotti, N. Li, M. J. T. Reinders, E. Eisemann, F. Koning, A. Vilanova, and B. P. F. Lelieveldt, "Visual analysis of mass cytometry data by hierarchical stochastic neighbour embedding reveals rare cell types," *Nature Communications*, vol. 8, no. 1, p. 1740, 2017.
- [40] G. C. Linderman, M. Rachh, J. G. Hoskins, S. Steinerberger, and Y. Kluger, "Fast interpolation-based t-SNE for improved visualization of single-cell RNA-seq data," *Nature Methods*, vol. 16, no. 3, pp. 243–245, 2019.
- [41] J. Yang and J. Leskovec, "Defining and evaluating network communities based on ground-truth," *Knowledge and Information Systems*, vol. 42, no. 1, pp. 181–213, 2015.

- [42] L. van der Maaten, "Learning a parametric embedding by preserving local structure," in *Proceedings of the 12th International Conference on Artificial Intelligence and Statistics*, vol. 5, 2009, pp. 384–391.
- [43] M. Muja and D. G. Lowe, "Scalable nearest neighbor algorithms for high dimensional data," *IEEE TPAMI*, vol. 36, no. 11, pp. 2227–2240, 2014.
- [44] —, "Fast approximate nearest neighbors with automatic algorithm configuration," in *International Conference on Computer Vision Theory and Application*. INSTICC Press, 2009, pp. 331–340.
- [45] T. U. Consortium, "Reorganizing the protein space at the Universal Protein Resource (UniProt)," *Nucleic Acids Research*, vol. 40, no. D1, pp. D71–D75, 2011.
- [46] M. Su, H. Zhang, X. Duy, and Q. Dai, "A novel stochastic-encryption-based P2P digital rights management scheme," in *IEEE International Conference on Communications*, 2015, pp. 5541–5545.
- [47] T. Liu and X. Sun, "Density-based detection of community hierarchy from graph description," 2019, manuscript in preparation.
- [48] "Transcriptional profiling of 1.3 million brain cells with the Chromium Single Cell 3' solution," 10x Genomics LIT000015 Chromium Million Brain Cells Application Note, 2017.
- [49] G. X. Y. Zheng, J. M. Terry, P. Belgrader, P. Ryvkin, Z. W. Bent, R. Wilson, S. B. Ziraldo, T. D. Wheeler, G. P. McDermott, J. Zhu, M. T. Gregory, J. Shuga, L. Montesclaros, J. G. Underwood, D. A. Masquelier, S. Y. Nishimura, M. Schnell-Levin, P. W. Wyatt, C. M. Hindson, R. Bharadwaj, A. Wong, K. D. Ness, L. W. Beppu, H. J. Deeg, C. McFarland, K. R. Loeb, W. J. Valente, N. G. Ericson, E. A. Stevens, J. P. Radich, T. S. Mikkelsen, B. J. Hindson, and J. H. Bielas, "Massively parallel digital transcriptional profiling of single cells," *Nature Communications*, vol. 8, p. 14049, 2017.
- [50] E. A. Abbott, *Flatland: A Romance of Many Dimensions*. London, UK: Seeley & Co, 1884.
- [51] J. Barnes and P. Hut, "A hierarchical  $O(N \log N)$  force-calculation algorithm," *Nature*, vol. 324, no. 6096, pp. 446–449, 1986.
- [52] L. Greengard and V. Rokhlin, "A fast algorithm for particle simulations," *Journal of Computational Physics*, vol. 73, no. 2, pp. 325–348, 1987.
- [53] X. Sun and N. P. Pitsianis, "A matrix version of the fast multipole method," *SIAM Review*, vol. 43, no. 2, pp. 289–300, 2001.
- [54] B. Zhang, J. Huang, N. P. Pitsianis, and X. Sun, "recFMM: Recursive parallelization of the adaptive fast multipole method for Coulomb and screened Coulomb interactions," *Communications in Computational Physics*, vol. 20, no. 2, pp. 534–550, 2016.
- [55] Y. Zhang, J. Liu, E. Kultursay, M. Kandemir, N. Pitsianis, and X. Sun, "Automatic parallel code generation for NuFFT data translation on multicores," *Journal of Circuits, Systems, and Computers*, vol. 21, no. 2, p. 1240004, 2012.
- [56] D. Floros, T. Liu, N. Pitsianis, and X. Sun, "Sparse dual of the density peaks algorithm for cluster analysis of high-dimensional data," in *IEEE High Performance Extreme Computing Conference*, 2018.
- [57] J. Mellor-Crummey, D. Whalley, and K. Kennedy, "Improving memory hierarchy performance for irregular applications using data and computation reorderings," *International Journal of Parallel Programming*, vol. 29, no. 3, pp. 217–247, 2001.
- [58] A. Buluç, J. T. Fineman, M. Frigo, J. R. Gilbert, and C. E. Leiserson, "Parallel sparse matrix-vector and matrix-transpose-vector multiplication using compressed sparse blocks," in *Proceedings of the 21st Annual Symposium on Parallelism in Algorithms and Architectures*, 2009, pp. 233–244.
- [59] R. D. Blumofe, C. F. Joerg, B. C. Kuszmaul, C. E. Leiserson, K. H. Randall, and Y. Zhou, "Cilk: An efficient multithreaded runtime system," *Journal of Parallel and Distributed Computing*, vol. 37, no. 1, pp. 55–69, 1996.
- [60] J. D. McCalpin, "Memory bandwidth and machine balance in current high performance computers," *IEEE Computer Society Technical Committee on Computer Architecture (TCAA) Newsletter*, 1995. [Online]. Available: <http://www.cs.virginia.edu/~mccalpin/papers/balance/>
- [61] D. A. Patterson and J. L. Hennessy, *Computer organization and design: the hardware/software interface*. Elsevier, 2014.
- [62] A. Yzelman and R. H. Bisseling, "Cache-oblivious sparse matrix-vector multiplication by using sparse matrix partitioning methods," *SIAM Journal on Scientific Computing*, vol. 31, no. 4, pp. 3128–3154, 2009.